Atmospheric Environment 120 (2015) 297–306

Contents lists available at ScienceDirect

Atmospheric Environment

journal homepage: www.elsevier.com/locate/atmosenv

Characterization of aerosol composition, concentrations, and sources at Baengnyeong Island, Korea using an aerosol mass spectrometer

Taehyoung Lee [a], Jinsoo Choi [c], Gangwoong Lee [a], Junyoung Ahn [c], Jin Soo Park [c], Samuel A. Atwood [b], Misha Schurman [b], Yongjoo Choi [a], Yoomi Chung [a], Jeffrey L. Collett Jr. [b, *]

[a] Department of Environmental Science, Hankuk University of Foreign Studies, Yongin, Republic of Korea
[b] Department of Atmospheric Science, Colorado State University, Fort Collins, USA
[c] Climate & Air Quality Research Department, National Institute of Environmental Research, Incheon, Republic of Korea

HIGHLIGHTS

- We measured the overall chemical properties of particulate matter at Baengnyeong Island, Korea.
- Organic matter and sulfate were the dominant chemical species in PM1.
- Observed organic aerosol was generally highly oxidized.
- Significant increases in sulfate concentration by transport from eastern China.
- Organic aerosol transported from both China and other regions of east Asia.

ARTICLE INFO

Article history:
Received 3 March 2015
Received in revised form
9 August 2015
Accepted 13 August 2015
Available online 22 August 2015

Keywords:
HR-ToF-AMS
Baengnyeong island
Long-range transport
Biomass burning
Potential source contribution

ABSTRACT

To improve understanding of the sources and chemical properties of particulate pollutants on the western side of the Korean Peninsula, an Aerodyne High Resolution Time of Flight Aerosol Mass Spectrometer (HR-ToF-AMS) measured non-refractory fine (PM_1) particles from May to November, 2011 at Baengnyeong Island, South Korea. Organic matter and sulfate were generally the most abundant species and exhibited maximum concentrations of 36 μg/m^3 and 39 μg/m^3, respectively. Nitrate concentrations peaked at 32 μg/m^3 but were typically much lower than sulfate and organic matter concentrations. May, September, October, and November featured the highest monthly average concentrations, with lower concentrations typically observed from June through August. Potential source contribution function (PSCF) analysis and individual case studies revealed that transport from eastern China, an area with high SO_2 emissions, was associated with high particulate sulfate concentrations at the measurement site. Observed sulfate aerosol sometimes was fully neutralized by ammonium but often was acidic; the average ammonium to sulfate molar ratio was 1.49. Measured species size distributions revealed a range of sulfate particle size distributions with modes between 100 and 600 nm. Organic aerosol source regions were widespread, including contributions from eastern China and South Korea. Positive matrix factorization (PMF) analysis indicated three "factors," or types of organic aerosol, comprising one primary, hydrocarbon-like organic aerosol (HOA) and two oxidized organic aerosol (OOA) components, including a more oxidized (MO-OOA) and a less oxidized (LO-OOA) oxidized organic aerosol. On average, HOA and OOA contributed 21% and 79% of the organic mass (OM), respectively, with the MO-OOA fraction nearly three times as abundant as the LO-OOA fraction. Biomass burning contributions to observed OM were low during the late spring/early summer agricultural burning season in eastern China, since airflow into eastern China during the Asian Monsoon generally prevents transport of emissions eastward to the Korean Peninsula. Concentrations of the *m/z* 60 AMS biomass burning marker were more abundant in autumn, when transport patterns appeared to bring some smoke from fires in northern Asia to the island.

* Corresponding author.
E-mail address: Collett@atmos.colostate.edu (J.L. Collett).

http://dx.doi.org/10.1016/j.atmosenv.2015.08.038
1352-2310/

1. Introduction

The issue of international transport of air pollutants in East Asia has been exacerbated by increased emissions of air pollutants produced by rapid industrial growth and automobiles in China and many Asian countries (Streets et al., 2001; Park and Lee, 2002; Richter et al., 2005). Although Chinese emissions of SO_2 dropped significantly from 1995 to 2000 (Carmichael et al., 2002), they resumed a rapid upward trend from 2000 to 2006, peaking at 34 Tg before dropping to 31 Tg in 2010 (Lu et al., 2011). The large SO_2 emissions reflect a heavy reliance on coal combustion for energy production and the high sulfur content of China's coal reserves (the average sulfur content is 1.1%, but reaches 4% in some regions) (Larssen et al., 2006). While flue gas desulfurization has resulted in rapid decreases in Chinese SO_2 emissions from the power generation sector, industrial SO_2 emissions have grown quickly (Lu et al., 2011). While Chinese air pollution problems have long been dominated by sulfur emissions, NO_x emissions are also rising rapidly. The annual growth rate of nitrogen dioxide (NO_2) concentrations over industrial areas in China increased by 50% during 1996–2004 (Richter et al., 2005), reflecting increased energy production and a rapid increase in the number of automobiles (Larssen et al., 2006).

These growing emissions are a concern within China and beyond. Since prevailing winds near the Korean Peninsula are often westerly, transport of air pollution from eastern China is a concern to South Korea and to more distant regions such as Japan and the western United States (Shim and Park, 2004; Kim et al., 2009).

Baengnyeong Island, Korea (see Fig. 1) is well-placed to investigate pollutant transport to the western side of the Korean Peninsula from a variety of source regions. Located in the sea west of the Korean Peninsula, approximately 180 km from the Chinese Shandong Peninsula, Baengnyeong Island is situated close to the North Korea–South Korea border. Under varying transport conditions, the island is strongly influenced by emissions from China, North Korea or South Korea. A comprehensive set of aerosol properties (PM_1, $PM_{2.5}$, and PM_{10}, OC, EC, metal concentrations, major ion concentrations, size distributions), including those from operation of an IMPROVE network sampler, and trace gas (O_3, NO_x, CO, CO_2, SO_2, and VOCs) concentrations is monitored routinely at the Baengyeong Island site by NIER (National Institute of Environmental Research) (Kim et al., 2011; Lee et al., 2012). Understanding air pollution source regions is critical to developing strategies to reduce regional air pollution, including concentrations of fine particles which impact human health, visibility, and climate forcing.

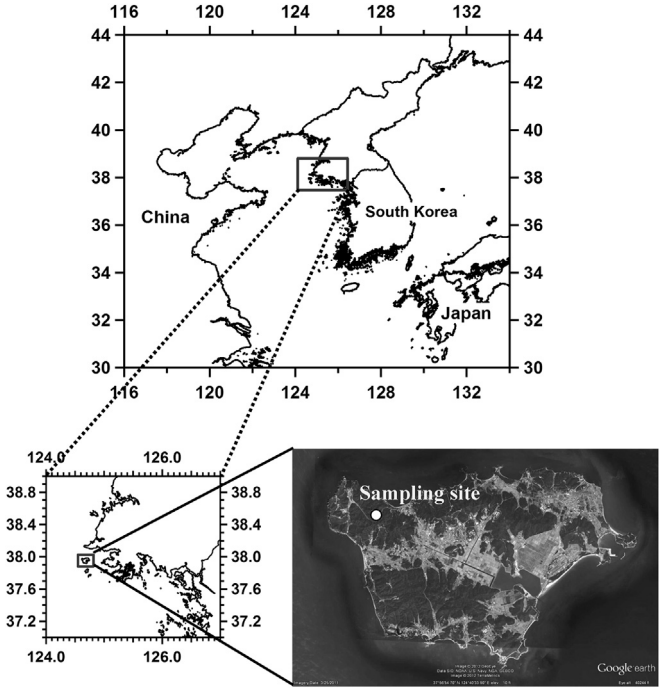

Fig. 1. Map of Korea showing the sampling location of Baengnyeong Island.

Given the rapid timescales common to changes in meteorology and transport, high time-resolution measurements of aerosol composition are valuable for understanding how changing transport influences local aerosol concentrations. The recently developed Aerodyne High-Resolution Time-of-Flight Aerosol Mass Spectrometer (hereafter, AMS) (DeCarlo et al., 2006; Canagaratna et al., 2007), was deployed at an air pollution monitoring site on Baengnyeong Island. A 7-month study was conducted from May to November, 2011, to provide insight into time varying, size-resolved, non-refractory fine particle composition, including concentrations of nitrate, sulfate, and organics. Analyses of these observations provide important insights into regional aerosol characteristics and to important source types and regions.

2. Methods

2.1. Sampling site and instrumentation

Field measurements were conducted during May–November 2011 at Baengnyeong Island, Korea (37.967 °N, 124.630 °E), located in the sea west of the Korean Peninsula approximately 180 km from the Shandong Peninsula in eastern China (Fig. 1), using an AMS. AMS measurements were conducted at an atmospheric research supersite (Baengnyeong Island Atmospheric Research Center) operated by the Korea National Institute of Environmental Research (NIER) and located at a hill approximately 100 m above sea level. The population on the island is small (~5000); the research center is located on the island's sparsely populated western side.

The operation of the AMS has been described in detail elsewhere (Jayne et al., 2000; Jimenez et al., 2003; DeCarlo et al., 2006; Drewnick et al., 2006), so only a brief summary is provided here. Ambient air was drawn through a URG cyclone (D_{50} = 2.5 μm, 3 LPM). Perma Pure dryers (MD-110-24) were used to control sample humidity (<40% RH), reducing uncertainties due to bounce-related changes in collection efficiency. Dried ambient air enters the AMS through a critical orifice (100 μm pin hole) and is focused into a narrow particle beam by an aerodynamic lens, after which the particles (1 μm size cut) are accelerated into the high-vacuum Particle Time-of-Flight (PToF) region. The AMS was operated under V-mode only. In this study, 5 min time resolution was used for determining particle composition, including concentrations of nitrate, sulfate, ammonium, and organic matter (The concentration of chloride (not shown) was also measured by the AMS). The AMS was calibrated for ionization efficiency (IE) through introduction of 350 nm ammonium nitrate particles. Relative ionization efficiencies for other aerosol types (sulfate, chloride, and organics) were taken from default values. PToF particle sizes were calibrated by introduction of a series of monodisperse aerosol standards (Polystyrene latex particles). A collection efficiency (CE) of 0.5 was used for the AMS quantitative analysis based on CE values observed in previous AMS campaigns and experiments under low humidity conditions (Middlebrook et al., 2011).

AMS data were analyzed using SQUIRREL and PIKA AMS data analysis software (DeCarlo et al., 2006; Sueper, 2009) in Igor Pro

(Wavemetrics Inc., v6.22). SQUIRREL version 1.50 was used to determine the mass concentration and chemically resolved size distribution of non-refractory PM_1. High resolution mass spectra were analyzed using PIKA version 1.10. V-mode spectra were analyzed to determine the elemental compositions of ion fragments (e.g. C_xH_y, $C_xH_yO_1$, and $C_xH_yO_z$), for PMF analysis, and for calculating Potential Source Contribution Functions (PSCF).

2.2. Positive matrix factorization analysis of AMS data set

The AMS aerosol mass spectra timeline was analyzed using Positive Matrix Factorization (PMF), a multivariate factor analysis tool (Paatero and Tapper, 1994; Paatero, 1997) previously applied to a wide range of data types, including 24-hr speciated $PM_{2.5}$, size-resolved aerosol, deposition, air toxics, and volatile organic compound (VOC) datasets (Poirot et al., 2001; Polissar et al., 2001; Kim et al., 2003; Kim and Hopke, 2004; Kim et al., 2004). Ulbrich et al. (2009) and others have previously applied PMF to AMS data, using the Igor Pro-based PMF evaluation tool (PET), also used here, which deconvolves unique spectral patterns, or 'factors' (such as hydrocarbon-like or biomass burning aerosol), from the mass spectra produced in each AMS run and constructs a representative spectrum and timeline of each factor (e.g. Lanz et al., 2007; Docherty et al., 2008; Ulbrich et al., 2009). Positive Matrix Factorization (PMF) was performed upon the V-mode AMS data after applying the error preparations outlined in SQUIRREL and PET. The method is described in greater detail elsewhere (Paatero and Tapper, 1994; Paatero, 1997; Ulbrich et al., 2009).

2.3. Back-trajectory residence time/potential source contribution function analyses

Backward-trajectory analysis was used to explore aerosol composition as a function of regional transport patterns. The NOAA HYSPLIT model (GDAS1 meteorological data set) was used to compute eight back-trajectories per day (3 h interval for each back-trajectory) for air masses arriving at the sampling site (37.967°N, 124.63°E) with receptor heights of 100 m and 1500 m. Back-trajectories were run for 120 h each between May and November 2011. Residence times and PSCF were determined by tracking trajectory endpoint locations within $1 \times 1^\circ$ grid cells every 60 min of transport time for the 100 m arrival height trajectories. Grid cells with less than 10 endpoints were screened from the results to reduce uncertainties in the analysis.

Residence time probability analysis (or residence time analysis; RTA) was used for interpreting back-trajectories to determine aerosol source regions. This method quantifies the relative impacts of source regions on the receptor site by calculating the previous positions of air parcels that arrived at the receptor over a specified time period. Regions containing more back-trajectory endpoints have a higher relative likelihood of transporting air to the receptor, allowing a spatial probability distribution map to be created that shows potentially important source regions. The mathematical details of RTA are extensively described in the literature and the method is well tested (Ashbaugh et al., 1985). The PSCF, originally proposed by Ashbaugh et al. (1985) and Malm et al. (1994), was developed from RTA and has been widely used to identify possible source areas for measured atmospheric constituents using back trajectories and concentration information. In PSCF analysis, the likelihood of a region containing a source for a particular constituent is estimated by looking at the percentage of back-trajectories that pass over that region which contain high concentrations of the constituent. In this case, concentrations higher than one standard deviation above the mean were classified as high concentration. The assumptions and mathematical approach of PSCF have been described in detail elsewhere (Liu et al., 2003; Begum et al., 2005; Sunder Raman and Hopke, 2007). PSCF was calculated for the entire study period (May–November, 2011).

3. Results and discussion

3.1. Submicron aerosol characteristics

A statistical summary of measured concentrations of PM_1 major species at Baengnyeong Island, by month, is presented in Table 1. Organic matter and sulfate were generally the most abundant aerosol components and exhibited maximum concentrations of 36 $\mu g/m^3$ and 39 $\mu g/m^3$, respectively. Nitrate concentrations peaked at 32 $\mu g/m^3$, but were typically much lower than sulfate and organic matter concentrations. The study average concentrations of organic matter, sulfate, and nitrate were 3.09, 4.32, and 0.89 $\mu g/m^3$, respectively. May, September, October, and November featured the highest monthly average concentrations of all three aerosol components, with lower concentrations observed from June through August.

Fig. 2a and b depict timelines of concentrations measured May–November, 2011. The relative mass fractions of the four measured PM_1 components are shown in Fig. 2c. The fractions of organic matter and sulfate range from 15 to 79% and 10–80%, respectively, while nitrate overall represents a minor fraction of PM_1. Sulfate and ammonium concentrations are strongly correlated ($R^2 = 0.85$) as shown in Fig. 3. The average aerosol at Baengnyeong Island was acidic, with an average PM_1 ammonium to sulfate molar ratio of 1.49 (standard deviation of 0.4), close to the molar ratio of letovicite. Observed variations in the ratio of ammonium to sulfate indicate that Baengnyeong Island sulfates usually correspond to a composition range between ammonium bisulfate (ratio = 1.0) and ammonium sulfate (ratio = 2.0). Ratios above 2 are expected when some of the ammonium is present as ammonium nitrate or ammonium salts of organic acids.

Table 1
Summary of the mass concentration ($\mu g/m^3$) of PM_1 major species measured using AMS during the 7-month study from May to November, 2011.

Species	Month	Average	Minimum	Maximum	STD
Organics	May	2.47	0.04	19.4	2.65
	June	2.11	0.06	10.4	1.57
	July	1.36	0.01	6.24	1.34
	August	1.62	0.01	8.78	1.61
	September	3.56	0.11	11.4	1.94
	October	5.84	0.36	24.01	3.63
	November	5.36	0.43	35.6	4.07
Sulfate	May	5.3	0.002	35.2	5.82
	June	4.43	0.01	18.3	3.29
	July	2.58	0.002	16.9	2.28
	August	2.74	0.001	22.9	2.72
	September	7.24	0.58	27.2	5.44
	October	5.04	0.28	28.9	5.55
	November	5.27	0.75	38.6	4.27
Nitrate	May	0.79	0.001	9.91	1.43
	June	0.62	0.005	7.95	0.91
	July	0.51	0.001	9.28	1.13
	August	0.32	0.002	5.71	0.6
	September	0.72	0.04	9.76	1.14
	October	1.47	0.03	12.7	1.73
	November	2.32	0.07	32.2	3.34
Ammonium	May	1.66	0.001	10.2	1.84
	June	1.21	0.05	4.61	0.87
	July	0.86	0.02	5.57	0.82
	August	0.85	0.003	5.69	0.74
	September	1.72	0.02	6.19	1.32
	October	1.66	0.11	10.5	1.73
	November	1.90	0.26	16.6	1.87

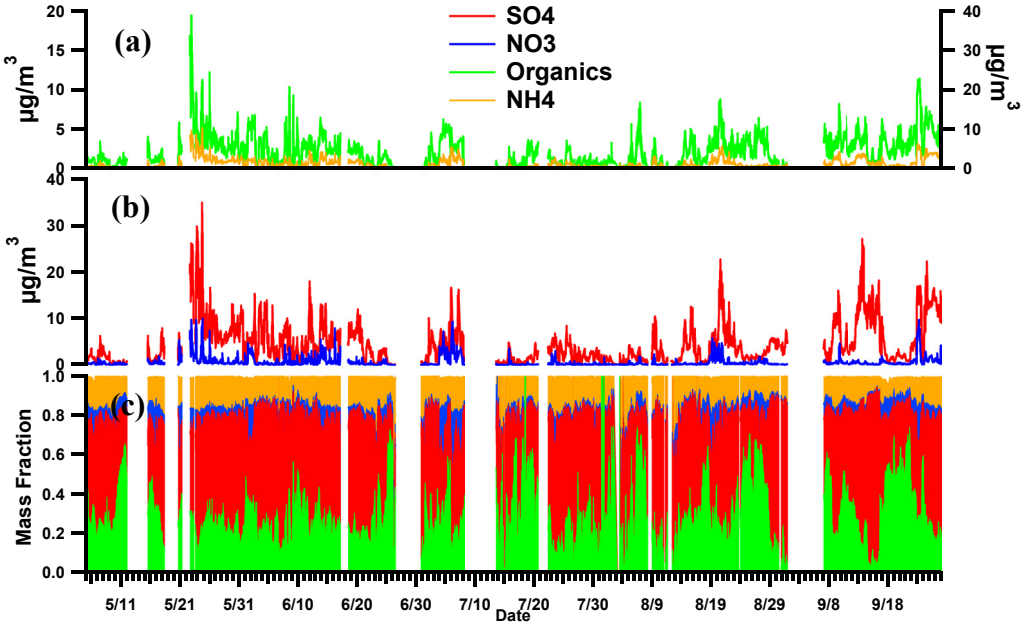

Fig. 2. Timelines of (a) organics and ammonium, (b) sulfate and nitrate concentrations, and (c) mass fractions of chemical species (organics, sulfate, nitrate, and ammonium) measured using AMS during May to November, 2011.

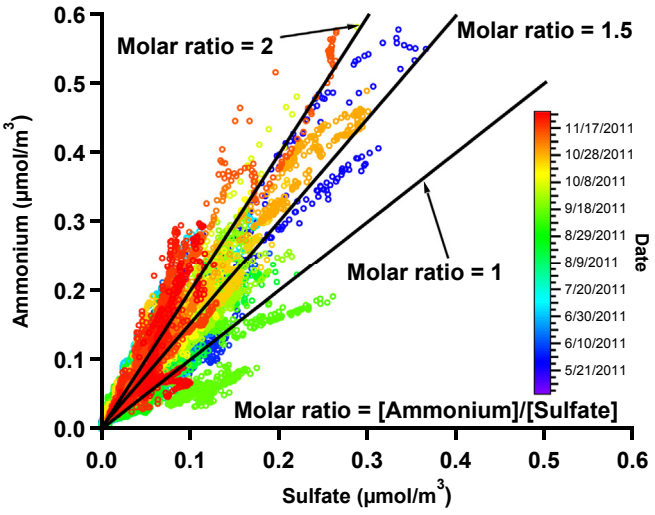

Fig. 3. Relationship between ammonium and sulfate concentrations in Baengnyeong Island fine particles. As reference, [ammonium]/[sulfate] molar ratios of 2.0, 1.5, and 1.0 are shown.

A main advantage of the high resolution AMS data is the separate quantification of different ions with the same nominal mass, enabling precise characterization of the elemental composition of each ion (e.g. $C_xH_y^+$, $C_xH_yO_1^+$, and $C_xH_yO_z^+$). This enhanced information is useful for understanding the overall chemical characteristics of ambient organic aerosols and their evolution in the atmosphere. Fig. 4 depicts timelines of contributions of three ion categories ($C_xH_y^+$, $C_xH_yO_1^+$, and $C_xH_yO_z^+$) of interest in organic aerosol (OA). Relative abundances of these fragments help describe the overall degree of OA oxidation. On average, the most oxidized fragment family ($C_xH_yO_z^+$) accounts for 42% of the three family sum, while the less oxidized $C_xH_yO_1^+$ family contributes 27%; 31% comes from the $C_xH_y^+$ family. The highest fractions of $C_xH_y^+$ are observed in autumn when decreased actinic fluxes reduce photochemical aging of atmospheric pollutants.

The evolution of OA can be seen more clearly in Fig. 5. The triangle region defined by two slopes of f_{44}: f_{43}, proposed by Ng et al. (2010), bounds values that typically describe the degree of ambient OA oxidation. The relative abundances of the OA fragment ions *m/z* 44 (CO_2^+) and *m/z* 43 ($C_2H_3O^+$) are key distinguishing characteristics of SV-OOA (semi-volatile oxygenated organic aerosol) and LV-OOA (low volatility oxygenated organic aerosol). SV-OOA f_{44}: f_{43} values tend to fall in the lower part of the triangle, while LV-OOA values tend to fall in the narrow region toward the top of the triangle. Fig. 5 shows f_{44}: f_{43} values for OA measured at Baengnyeong Island. Most of the values fall in the upper region of the triangle, suggesting that the observed OA is strongly aged/oxidized and likely to bear a strong resemblance to LV-OOA previously reported in other environments (Jimenez et al., 2009; Huang et al., 2010; Ng et al., 2010, 2011; Sun et al., 2011a; Sun et al., 2011b; Zhang et al., 2011).

3.2. Positive matrix factorization (PMF) analysis of AMS data set

PMF analysis of Baengnyeong Island AMS observations yielded factors similar to those observed in other rural environments. Hydrocarbon-like OA (HOA) (21% of apportioned OM) and oxygenated OA (OOA) (79% of apportioned OM) were both resolved. The three-factor solution was selected based on meaningful dissimilarities in average mass spectra, the time series of factors (not shown), and the Q value (or PMF quality-of-fit parameter) (not shown, Q/Q_{exp}~3 in this study) (Ulbrich et al., 2009; Zhang et al., 2011). A three factor solution resolved HOA, along with two OOA-like factors. Consistent with recent approaches in the literature (Hildebrandt et al., 2010; Zhang et al., 2011) we refer to these factors as more oxidized and less oxidized OOA (MO-OOA and LO-OOA). MO-OOA accounted, on average, for 58% of apportioned OM while LO-OOA accounted for 21%.

Mass spectra for the three PMF factors are included in Fig. 6. The HOA component is distinguished by the clear hydrocarbon signature in its spectrum at *m/z* 41, 43, and 55, consistent with previous studies (Hildebrandt et al., 2010; Ng et al., 2010, 2011). The LO-OOA

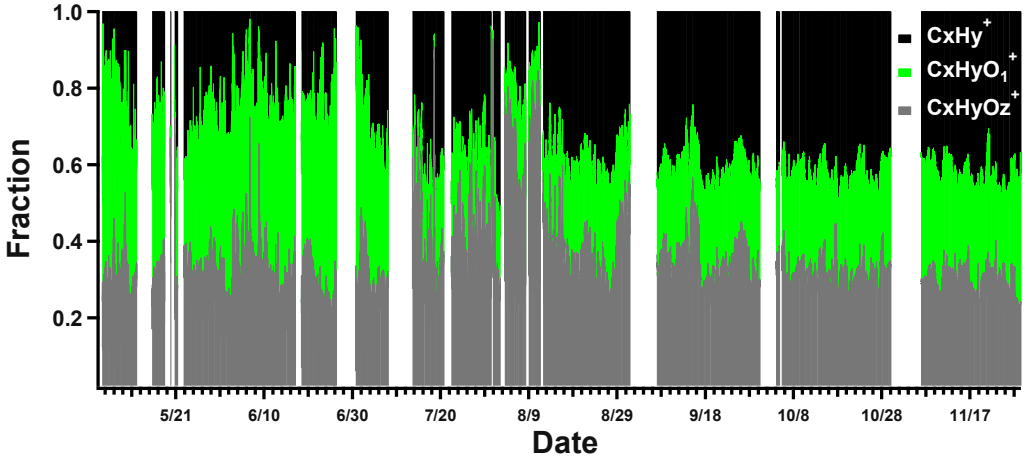

Fig. 4. Timelines of contribution of OA components to three ion categories ($C_xH_y^+$, $C_xH_yO_1^+$, and $C_xH_yO_z^+$) from May to November, 2011.

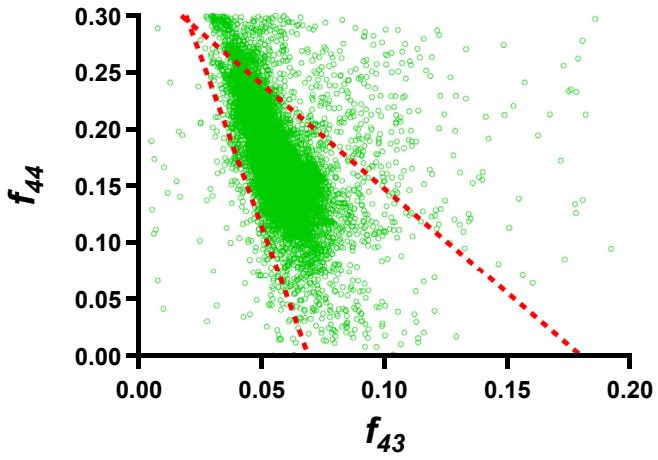

Fig. 5. Relationship between f_{44} (fraction of m/z 44 to total organics concentration) and f_{43} (fraction of m/z 43 to total organics concentration) during the entire study. The triangle region is defined by two different slopes of f_{44} and f_{43} as described by Ng et al. (2010).

factor has fractional m/z 44 (f_{44}) of 13% and fractional m/z 43 (f_{43}) of 6%, similar to typical LV-OOA factors based on aerosol volatility (f_{44} = 12–15%, f_{43} = 5–7%) determined in previous studies (e.g. (Hildebrandt et al., 2010; Ng et al., 2010, 2011; Zhang et al., 2011). The MO-OOA factor is distinguished by a much higher fraction of m/z 44 (f_{44} = 25.6%) than seen in LO-OOA, similar to aged aerosol observed by Hildebrandt et al. (2010).

Modest diurnal trends in MO-OOA and LO-OOA abundance are apparent (see Fig. 7). While MO-OOA increases from mid-morning through late afternoon then decreases slowly overnight, LO-OOA increases from early morning through midday then decreases strongly through early afternoon then more slowly into the evening. The diurnal variation of MO-OOA shows similarities to sulfate (not shown here), suggesting these patterns are of a possible formation of LO-OOA early in the day paired with an LO-OOA to MO-OOA photochemical conversion in the afternoon, although it is possible that other factors (e.g. transport and changes in boundary layer depth, MO-OOA formation via cloud photochemical processing) also influence the observed diurnal trends.

Mass fragments m/z 60 and m/z 73 are commonly used as markers for biomass burning in AMS observations (Schneider et al., 2006; Alfarra et al., 2007; Weimer et al., 2008; Mohr et al., 2009; Lee et al., 2010; Cubison et al., 2011). In this study biomass burning organic aerosol (BBOA) concentrations were too low to be resolved as a distinct factor in PMF analysis (f_{60} = 0.9% in the LO-OOA factor and f_{60} amounts were negligible in the HOA and MO-OOA factors). The fraction of m/z 44 suggests a range of degrees of oxidation in the measured OA, with values commonly between 10% and 30% (Fig. S1). Multiple previous studies have observed that m/z 60 is present at a level of ~0.3% of total OA during periods

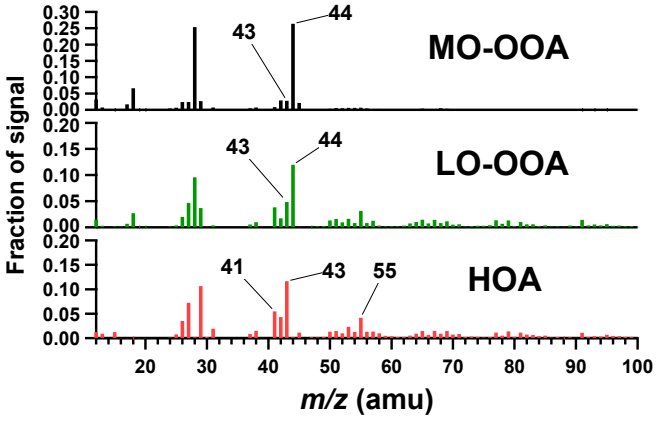

Fig. 6. The mass spectra of three OA factors determined on the basis of PMF analysis of the AMS data from May to November, 2011.

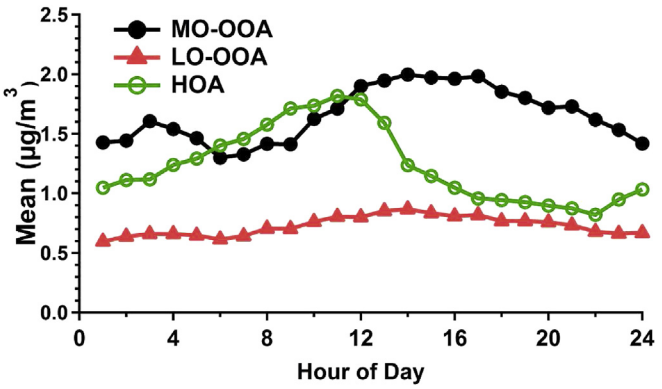

Fig. 7. Average diurnal trends of LO-OOA, MO-OOA, and HOA.

without biomass burning influence (Docherty et al., 2008; Aiken et al., 2009; Cubison et al., 2011). The Baengnyeong Island AMS measurements exhibit a small range of f_{60}, approximately 0.1–0.6% of total OA (average ~0.2%) (Fig. S1). Higher f_{60} values (more than ~0.3%) were observed in late October and early November, suggesting a possible biomass burning source influence during that period.

3.3. Residence time analysis (RTA) and potential source contribution function (PSCF) analysis

A back-trajectory RTA for June, shown in Fig. S2, suggests that despite extensive prescribed burning in eastern China (Fig. S3) (Yamaji et al., 2010), emissions from this region did not strongly impact Baengnyeong Island, consistent with the lack of f_{60} enhancement above background (Fig. S1). Air masses reaching the island in June passed through the southeastern part of the China Sea (west of Korea). In contrast, air masses reaching Baengnyeong Island in late October and early November arrived frequently from eastern and northeastern China (Fig. 8 and Fig. S2). Higher concentrations of mass fragment *m/z* 60 observed with the AMS during this period are consistent with transport of biomass burning emissions from observed fires in these regions (Fig. S4).

Trends in sulfate aerosol loading are also consistent with RTA findings (Fig. S2) and SO_2 spatial emissions in China (Fig. S5). During the highest sulfate concentration periods (May, September, and August), air masses arriving at Baengnyeong Island frequently spent time over east/northeast China, suggesting that high sulfate concentrations at Baengnyeong Island during these timeframes often result from high SO_2 emissions in China. This can be seen more clearly in Fig. 9, which shows PSCF analyses of fine particle sulfate and organics. The PSCF analyses show higher percentages of air masses passing over this region to be associated with higher concentrations of these species at the receptor. The presented findings, averaged over the course of the study, reveal associations between transport from particular regions and high fine particle sulfate or organic concentrations observed at Baengnyeong Island. For sulfate aerosol, PSCF analysis identified source areas throughout east/northeast China (Fig. 9a), consistent with the aging of abundant SO_2 emissions from this region. East/northeast and northern China appear as important source regions of organic aerosol from anthropogenic emissions/biomass burning and biomass burning, respectively, although PSCF analysis also suggests important OA contributions from other parts of East Asia including South Korea (Fig. 9b).

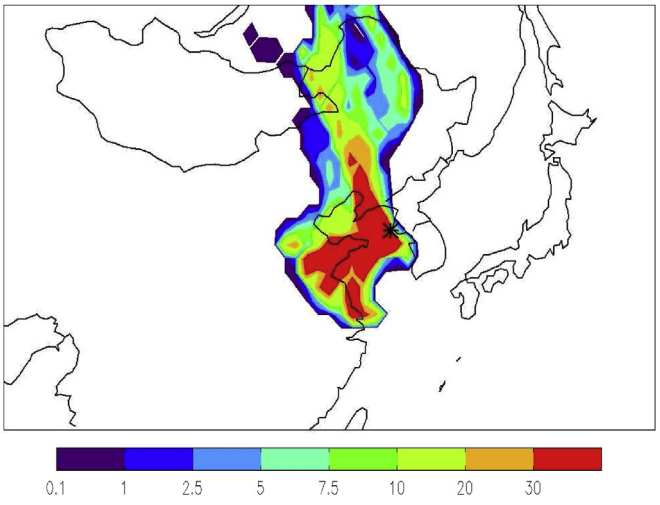

Fig. 8. The 120-hr back trajectory residence time analysis for 10/25–11/10, 2011. Contoured lines indicate the residence time as a percentage of the maximum residence time of air parcels in any 1 × 1 degree box.

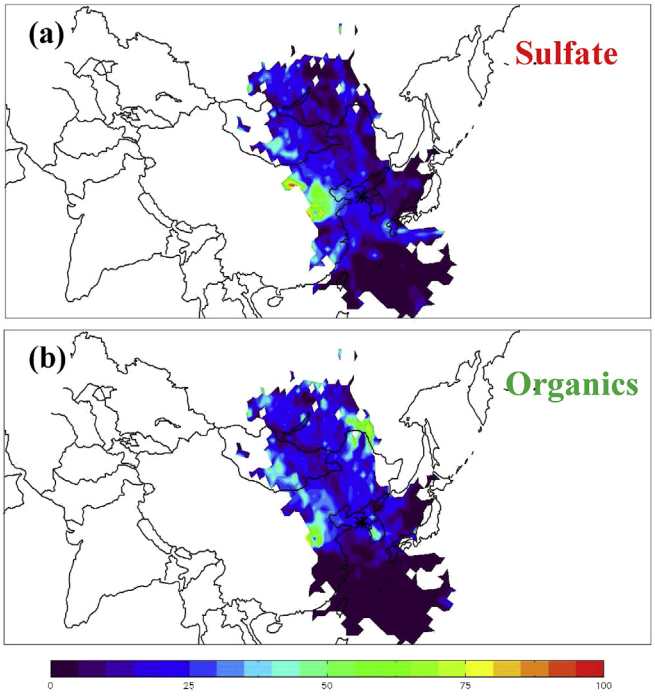

Fig. 9. Potential Source Contribution Function (PSCF) map indicating the conditional probability that an air parcel passing over a region arrived at Baengnyeong Island with a high concentration of (a) sulfates or (b) organics measured during May through November, 2011. The scale shows the conditional probability as percentage likelihood.

3.4. Case studies

In order to gain further insight into the relationship between transport and aerosol characteristics at Baengnyeong Island, a series of case studies was considered. Figs. 10–12 show the average size distributions and timelines of PM_1 chemical composition for periods of contrasting long range transport. Case I (Fig. 10) contrasts two May time periods showing transport from China (May 23–24) and South Korea (May 28). Case II (Fig. 11) examines three September time periods with transport from the Korean Peninsula (Sept. 7), from eastern China (Sept. 13) and from the north (Sept. 19–20). Case III (Fig. 12) compares several August periods with transport from the East China Sea (Aug. 4 and 11), from eastern China (Aug. 20), and from the east and across South Korea (Aug. 27–28).

Aerosols transported from China exhibit different size distributions for different chemical constituents. Fig. 10b shows that the size distribution of sulfate peaks at a significantly smaller size than the size distributions for nitrate and organics. Fig. 11b, by contrast, shows a sulfate size distribution peaking at a significantly larger size than the size distributions for nitrate and organics. Both cases suggest that aerosols arriving from China on these dates are externally mixed. The sulfate size distribution peaks between 300 and 400 nm (D_{va}) in the May 23–24 case while the peak on September 13 is between 500 and 600 nm (D_{va}). These differences may reflect different oxidation mechanisms. Homogeneous gas phase oxidation of sulfur dioxide tends to produce smaller sulfate aerosol particles than are produced by aqueous phase oxidation in clouds (Seinfeld and Pandis, 2006). Cloud cover IR images from COMS (Communication, Ocean and Meteorological Satellite, http://

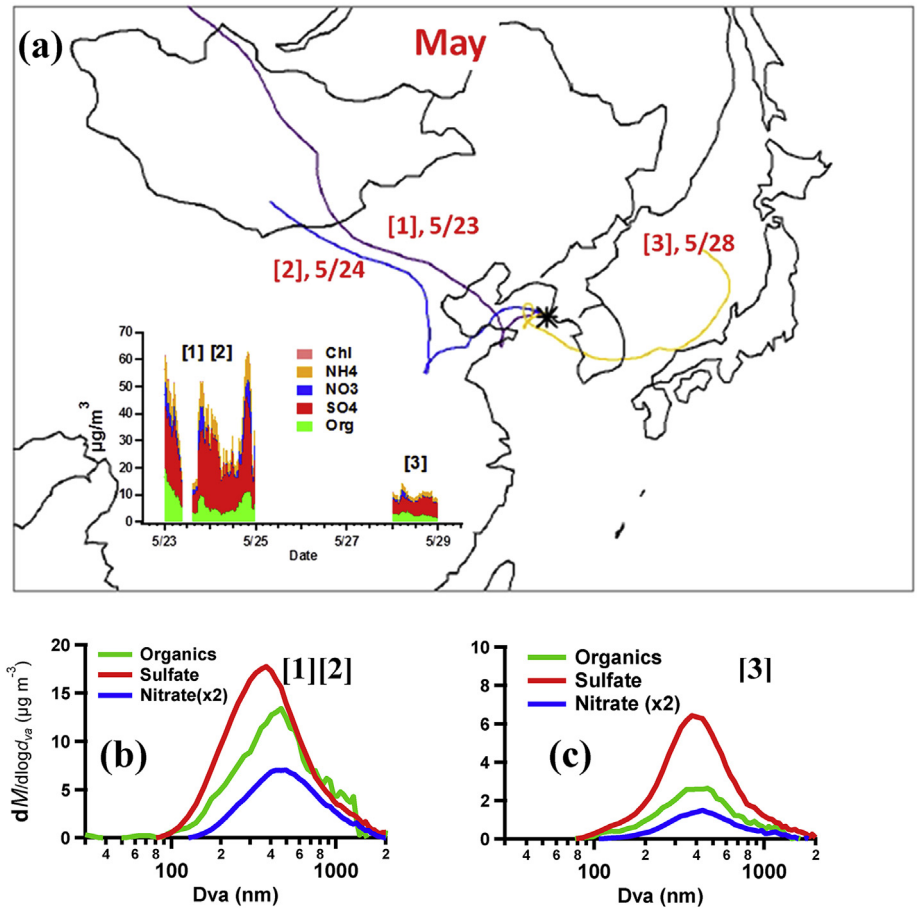

Fig. 10. (a) Case Study I back trajectories of air masses arriving at Baengnyeong Island and corresponding time series of PM_1 composition, (b) chemically-resolved size distributions of PM_1 measured from May 23–24, and (c) chemically-resolved size distributions of PM_1 observed during May 28.

nmsc.kma.go.kr) shown in Figs. S6–S8, suggest more cloud processing for sulfate in the September 13 observations (Fig. S6), when larger sulfate particles were observed, than in observations from May 23 (Fig. S7) and 24 (Fig. S8) when smaller sulfate particles were measured. While there was significant cloud on September 13 at 09:00 am, no cloud cover was observed on May 23 from early morning to late afternoon and clouds developed on May 24. Aerosol mode size can also grow as aerosol mass concentrations increase. This was clearly not the major factor here, however, since fine particle concentrations observed on May 23–24 were similar to or higher than those observed on September 13.

Similar size distributions of sulfate, nitrate, and organics in aerosols transported across the Korean Peninsula (Figs. 10c and 11c) suggest these aerosols may be internally mixed. Further information is required to test this possibility. Interestingly, the size distributions of nitrate and organics are fairly similar, peaking at approximately 400–500 nm (D_{va}), whether air masses arrived from China or across the Korean Peninsula.

The inset concentration timelines in Figs. 10–12 show that most significant sulfate concentration increases are associated with arrival of air masses from China; changes in organic matter concentration are not as large and not clearly tied to changes in transport. These case study observations are consistent with the PSCF analysis presented above, which indicates a major source region for sulfate in eastern China with more distributed organic aerosol source regions. As seen in Fig. 12 for August 4 and August 11, trajectories that bring air from the south through the East China Sea without crossing major land-based source regions often contain low fine particle concentrations of sulfate, nitrate, and organics.

4. Conclusions

The chemical composition of non-refractory submicron particles was measured at an air quality supersite on Baengnyeong Island during May–November, 2011. The highest monthly average concentrations of PM_1 were observed in May and in September through November. Organic matter and sulfate were the dominant chemical species observed in PM_1 during this time period, together comprising on average approximately 80% of total non-refractory PM_1 measured by the AMS. Sulfate aerosol was typically moderately acidic, with an average ammonium to sulfate molar ratio of 1.49.

Observed organic aerosol at Baengnyeong Island was generally highly oxidized. Three organic aerosol PMF component factors were determined. HOA and OOA were determined to constitute, on average, 21% and 79%, of the total organic aerosol. The OOA factor contained MO-OOA and LO-OOA components. MO-OOA was typically much more abundant than LO-OOA. AMS measurements during the study exhibited a small range of f_{60}, ranging mostly from 0.1% to 0.6% of total OA. Higher f_{60} values were frequently observed in late October and November, associated with apparent transport of biomass burning emissions from prescribed burning in eastern and northeastern China.

RTA and PSCF analysis, combining back-trajectory analysis and measured aerosol concentrations, helped determine source regions of Baengnyeong Island aerosol. These analyses were also

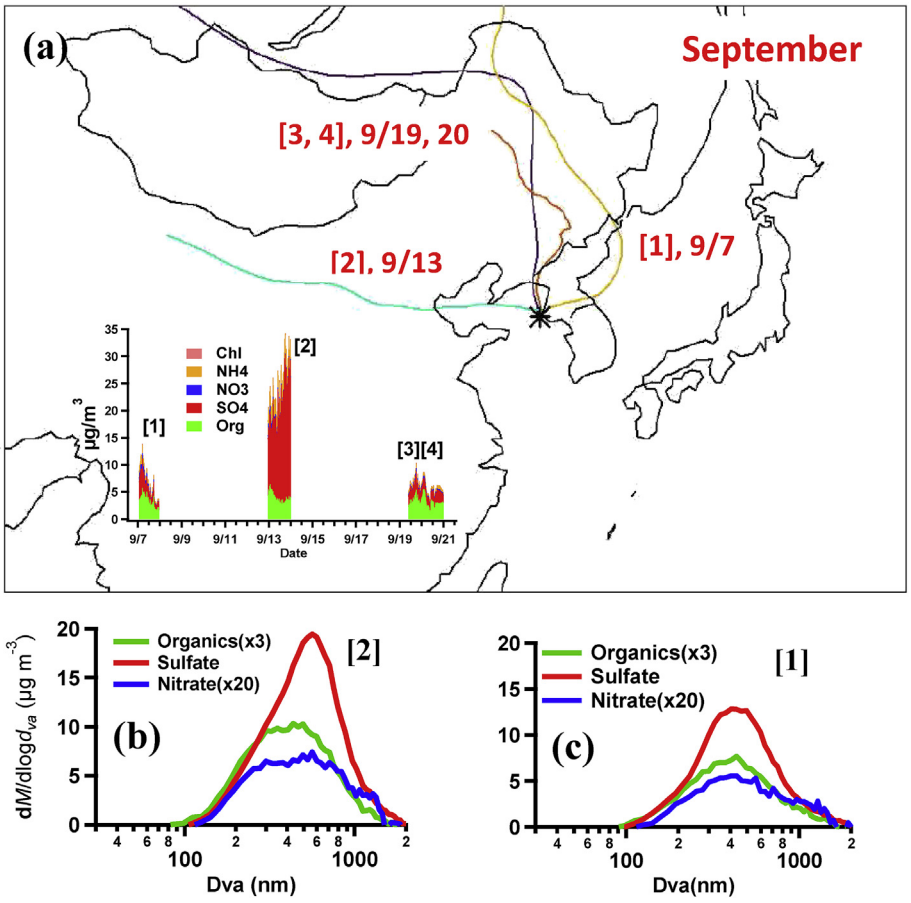

Fig. 11. (a) Case Study II back trajectories of air masses arriving at Baengnyeong Island and corresponding time series of PM_1 composition, (b) chemically-resolved size distributions of PM_1 measured September 19, and (c) chemically-resolved size distributions of PM_1 observed September 7.

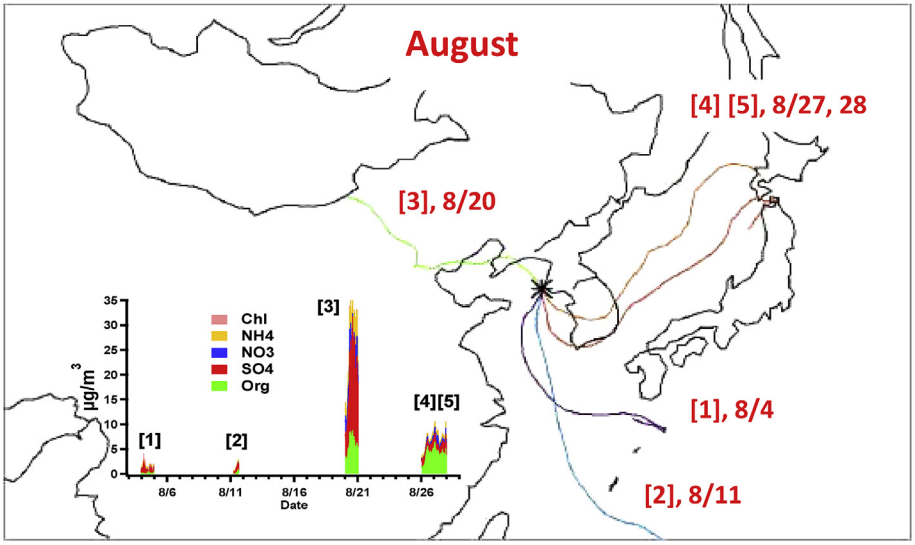

Fig. 12. Case Study III back trajectories of air masses arriving at Baengnyeong Island and corresponding time series of PM_1.

complemented by several case studies. Significant increases in sulfate concentration were typically associated with long-range transport from eastern China. Organic matter concentrations at the site, however, were influenced by transport from both China and other regions of East Asia, including South Korea. Particle size distributions of individual chemical components measured during periods of transport from China revealed different sizes for organic matter and nitrate than for sulfate, suggesting an externally mixed particle population. During periods of likely cloud processing, sulfate particles were larger than nitrate and organic particles,

consistent with formation of a sulfate "droplet mode". During periods when cloud processing was less likely, sulfate particles were smaller than organic and nitrate particles.

Acknowledgments

The authors thank the research scientists at Baengnyeong Island and the Climate & Air Quality Research Department, National Institute of Environmental Research (Korea) for their contributions to the success of the field campaign. This study was supported by a Grant from the National Research Foundation of Korea (NRF-2014R1A1A1007947).

Appendix A. Supplementary data

Supplementary data related to this article can be found at http://dx.doi.org/10.1016/j.atmosenv.2015.08.038.

References

Aiken, A.C., Salcedo, D., Cubison, M.J., Huffman, J.A., DeCarlo, P.F., Ulbrich, I.M., Docherty, K.S., Sueper, D., Kimmel, J.R., Worsnop, D.R., Trimborn, A., Northway, M., Stone, E.A., Schauer, J.J., Volkamer, R.M., Fortner, E., de Foy, B., Wang, J., Laskin, A., Shutthanandan, V., Zheng, J., Zhang, R., Gaffney, J., Marley, N.A., Paredes-Miranda, G., Arnott, W.P., Molina, L.T., Sosa, G., Jimenez, J.L., 2009. Mexico City aerosol analysis during MILAGRO using high resolution aerosol mass spectrometry at the urban supersite (T0) – Part 1: fine particle composition and organic source apportionment. Atmos. Chem. Phys. 9, 6633–6653.

Alfarra, M.R., Prevot, A.S.H., Szidat, S., Sandradewi, J., Weimer, S., Lanz, V.A., Schreiber, D., Mohr, M., Baltensperger, U., 2007. Identification of the mass spectral signature of organic aerosols from wood burning emissions. Environ. Sci. Technol. 41, 5770–5777.

Ashbaugh, L.L., Malm, W.C., Sadeh, W.Z., 1985. A residence time probability analysis of sulfur concentrations at grand-Canyon-National-Park. Atmos. Environ. 19, 1263–1270.

Begum, B.A., Kim, E., Jeong, C.-H., Lee, D.-W., Hopke, P.K., 2005. Evaluation of the potential source contribution function using the 2002 Quebec forest fire episode. Atmos. Environ. 39, 3719–3724.

Canagaratna, M.R., Jayne, J.T., Jimenez, J.L., Allan, J.D., Alfarra, M.R., Zhang, Q., Onasch, T.B., Drewnick, F., Coe, H., Middlebrook, A., Delia, A., Williams, L.R., Trimborn, A.M., Northway, M.J., DeCarlo, P.F., Kolb, C.E., Davidovits, P., Worsnop, D.R., 2007. Chemical and microphysical characterization of ambient aerosols with the aerodyne aerosol mass spectrometer. Mass Spectrom. Rev. 26, 185–222.

Carmichael, G.R., Streets, D.G., Calori, G., Amann, M., Jacobson, M.Z., Hansen, J., Ueda, H., 2002. Changing trends in sulfur emissions in Asia: implications for acid deposition, air pollution, and climate. Environ. Sci. Technol. 36, 4707–4713.

Cubison, M.J., Ortega, A.M., Hayes, P.L., Farmer, D.K., Day, D., Lechner, M.J., Brune, W.H., Apel, E., Diskin, G.S., Fisher, J.A., Fuelberg, H.E., Hecobian, A., Knapp, D.J., Mikoviny, T., Riemer, D., Sachse, G.W., Sessions, W., Weber, R.J., Weinheimer, A.J., Wisthaler, A., Jimenez, J.L., 2011. Effects of aging on organic aerosol from open biomass burning smoke in aircraft and laboratory studies. Atmos. Chem. Phys. 11, 12049–12064.

DeCarlo, P.F., Kimmel, J.R., Trimborn, A., Northway, M.J., Jayne, J.T., Aiken, A.C., Gonin, M., Fuhrer, K., Horvath, T., Docherty, K.S., Worsnop, D.R., Jimenez, J.L., 2006. Field-deployable, high-resolution, time-of-flight aerosol mass spectrometer. Anal. Chem. 78, 8281–8289.

Docherty, K.S., Stone, E.A., Ulbrich, I.M., DeCarlo, P.F., Snyder, D.C., Schauer, J.J., Peltier, R.E., Weber, R.J., Murphy, S.M., Seinfeld, J.H., Grover, B.D., Eatough, D.J., Jimenez, J.L., 2008. Apportionment of primary and secondary Organic Aerosols in Southern California during the 2005 study of organic Aerosols in Riverside (SOAR-1). Environ. Sci. Technol. 42, 7655–7662.

Drewnick, F., Hings, S.S., Curtius, J., Eerdekens, G., Williams, J., 2006. Measurement of fine particulate and gas-phase species during the New Year's fireworks 2005 in Mainz, Germany. Atmos. Environ. 40, 4316–4327.

Hildebrandt, L., Engelhart, G.J., Mohr, C., Kostenidou, E., Lanz, V.A., Bougiatioti, A., DeCarlo, P.F., Prevot, A.S.H., Baltensperger, U., Mihalopoulos, N., Donahue, N.M., Pandis, S.N., 2010. Aged organic aerosol in the Eastern Mediterranean: the Finokalia aerosol measurement experiment-2008. Atmos. Chem. Phys. 10, 4167–4186.

Huang, X.F., He, L.Y., Hu, M., Canagaratna, M.R., Sun, Y., Zhang, Q., Zhu, T., Xue, L., Zeng, L.W., Liu, X.G., Zhang, Y.H., Jayne, J.T., Ng, N.L., Worsnop, D.R., 2010. Highly time-resolved chemical characterization of atmospheric submicron particles during 2008 Beijing Olympic Games using an Aerodyne High-Resolution Aerosol Mass Spectrometer. Atmos. Chem. Phys. 10, 8933–8945.

Jayne, J.T., Leard, D.C., Zhang, X.F., Davidovits, P., Smith, K.A., Kolb, C.E., Worsnop, D.R., 2000. Development of an aerosol mass spectrometer for size and composition analysis of submicron particles. Aerosol Sci. Technol. 33, 49–70.

Jimenez, J.L., Canagaratna, M.R., Donahue, N.M., Prevot, A.S.H., Zhang, Q., Kroll, J.H., DeCarlo, P.F., Allan, J.D., Coe, H., Ng, N.L., Aiken, A.C., Docherty, K.S., Ulbrich, I.M., Grieshop, A.P., Robinson, A.L., Duplissy, J., Smith, J.D., Wilson, K.R., Lanz, V.A., Hueglin, C., Sun, Y.L., Tian, J., Laaksonen, A., Raatikainen, T., Rautiainen, J., Vaattovaara, P., Ehn, M., Kulmala, M., Tomlinson, J.M., Collins, D.R., Cubison, M.J., Dunlea, E.J., Huffman, J.A., Onasch, T.B., Alfarra, M.R., Williams, P.I., Bower, K., Kondo, Y., Schneider, J., Drewnick, F., Borrmann, S., Weimer, S., Demerjian, K., Salcedo, D., Cottrell, L., Griffin, R., Takami, A., Miyoshi, T., Hatakeyama, S., Shimono, A., Sun, J.Y., Zhang, Y.M., Dzepina, K., Kimmel, J.R., Sueper, D., Jayne, J.T., Herndon, S.C., Trimborn, A.M., Williams, L.R., Wood, E.C., Middlebrook, A.M., Kolb, C.E., Baltensperger, U., Worsnop, D.R., 2009. Evolution of organic aerosols in the atmosphere. Science 326, 1525–1529.

Jimenez, J.L., Jayne, J.T., Shi, Q., Kolb, C.E., Worsnop, D.R., Yourshaw, I., Seinfeld, J.H., Flagan, R.C., Zhang, X., Smith, K.A., Morris, J.W., Davidovits, P., 2003. Ambient aerosol sampling using the Aerodyne aerosol mass spectrometer. J. Geophys. Res. Atmos. 108, 8425.

Kim, E., Hopke, P.K., 2004. Improving source identification of fine particles in a rural northeastern U.S. area utilizing temperature-resolved carbon fractions. J. Geophys. Res. 109, D09204.

Kim, E., Hopke, P.K., Edgerton, E.S., 2003. Source identification of Atlanta aerosol by positive matrix factorization. J. Air & Waste Manag. Assoc. 53, 731–739.

Kim, E., Hopke, P.K., Edgerton, E.S., 2004. Improving source identification of Atlanta aerosol using temperature resolved carbon fractions in positive matrix factorization. Atmos. Environ. 38, 3349–3362.

Kim, J.H., Yum, S.S., Shim, S., Yoon, S.C., Hudson, J.G., Park, J., Lee, S.J., 2011. On aerosol hygroscopicity, cloud condensation nuclei (CCN) spectra and critical supersaturation measured at two remote islands of Korea between 2006 and 2009. Atmos. Chem. Phys. 11, 12627–12645.

Kim, Y.J., Woo, J.-H., Ma, Y.-I., Kim, S., Nam, J.S., Sung, H., Choi, K.-C., Seo, J., Kim, J.S., Kang, C.-H., Lee, G., Ro, C.-U., Chang, D., Sunwoo, Y., 2009. Chemical characteristics of long-range transport aerosol at background sites in Korea. Atmos. Environ. 43, 5556–5566.

Lanz, V.A., Alfarra, M.R., Baltensperger, U., Buchmann, B., Hueglin, C., Prevot, A.S.H., 2007. Source apportionment of submicron organic aerosols at an urban site by factor analytical modelling of aerosol mass spectra. Atmos. Chem. Phys. 7, 1503–1522.

Larssen, T., Lydersen, E., Tang, D.G., He, Y., Gao, J.X., Liu, H.Y., Duan, L., Seip, H.M., Vogt, R.D., Mulder, J., Shao, M., Wang, Y.H., Shang, H., Zhang, X.S., Solberg, S., Aas, W., Okland, T., Eilertsen, O., Angell, V., Liu, Q.R., Zhao, D.W., Xiang, R.J., Xiao, J.S., Luo, J.H., 2006. Acid rain in China. Environ. Sci. Technol. 40, 418–425.

Lee, G., Choi, H.-S., Lee, T., Choi, J., Park, J.S., Ahn, J.Y., 2012. Variations of regional background peroxyacetyl nitrate in marine boundary layer over Baengyeong Island, South Korea. Atmos. Environ. 61, 533–541.

Lee, T., Sullivan, A.P., Mack, L., Jimenez, J.L., Kreidenweis, S.M., Onasch, T.B., Worsnop, D.R., Malm, W., Wold, C.E., Hao, W.M., Collett, J.L., 2010. Chemical smoke marker emissions during flaming and smoldering phases of laboratory open burning of wildland fuels. Aerosol Sci. Technol. 44, I–V.

Liu, W., Hopke, P.K., Han, Y.-j., Yi, S.-M., Holsen, T.M., Cybart, S., Kozlowski, K., Milligan, M., 2003. Application of receptor modeling to atmospheric constituents at Potsdam and Stockton, NY. Atmos. Environ. 37, 4997–5007.

Lu, Z., Zhang, Q., Streets, D.G., 2011. Sulfur dioxide and primary carbonaceous aerosol emissions in China and India, 1996–2010. Atmos. Chem. Phys. 11, 9839–9864.

Malm, W.C., Sisler, J.F., Huffman, D., Eldred, R.A., Cahill, D.M., 1994. Spatial and seasonal trends in particle concentration and optical extinction in the United States. J. Geophys. Res. 99, 1347–1370.

Middlebrook, A.M., Bahreini, R., Jimenez, J.L., Canagaratna, M.R., 2011. Evaluation of composition-dependent collection efficiencies for the Aerodyne aerosol mass spectrometer using field data. Aerosol Sci. Technol. 46, 258–271.

Mohr, C., Huffman, J.A., Cubison, M.J., Aiken, A.C., Docherty, K.S., Kimmel, J.R., Ulbricht, I.M., Hannigan, M., Jimenez, J.L., 2009. Characterization of primary organic aerosol emissions from meat cooking, trash burning, and motor vehicles with high-resolution aerosol mass spectrometry and comparison with ambient and chamber observations. Environ. Sci. Technol. 43, 2443–2449.

Ng, N.L., Canagaratna, M.R., Jimenez, J.L., Zhang, Q., Ulbrich, I.M., Worsnop, D.R., 2011. Real-time methods for estimating organic component mass concentrations from aerosol mass spectrometer data. Environ. Sci. Technol. 45, 910–916.

Ng, N.L., Canagaratna, M.R., Zhang, Q., Jimenez, J.L., Tian, J., Ulbrich, I.M., Kroll, J.H., Docherty, K.S., Chhabra, P.S., Bahreini, R., Murphy, S.M., Seinfeld, J.H., Hildebrandt, L., Donahue, N.M., DeCarlo, P.F., Lanz, V.A., Prevot, A.S.H., Dinar, E., Rudich, Y., Worsnop, D.R., 2010. Organic aerosol components observed in Northern Hemispheric datasets from Aerosol Mass Spectrometry. Atmos. Chem. Phys. 10, 4625–4641.

Paatero, P., 1997. Least squares formulation of robust non-negative factor analysis. Chemom. Intell. Lab. Syst. 37, 23–35.

Paatero, P., Tapper, U., 1994. Positive matrix factorization: a non-negative factor model with optimal utilization of error estimates of data values. Environmetrics 5, 111–126.

Park, S.-U., Lee, Y.-H., 2002. Spatial distribution of wet deposition of nitrogen in South Korea. Atmos. Environ. 36, 619–628.

Poirot, R.L., Wishinski, P.R., Hopke, P.K., Polissar, A.V., 2001. Comparative application of multiple receptor methods to identify aerosol sources in northern Vermont. Environ. Sci. Technol. 35, 4622–4636.

Polissar, A.V., Hopke, P.K., Poirot, R.L., 2001. Atmospheric aerosol over Vermont: chemical composition and sources. Environ. Sci. Technol. 35, 4604–4621.

Richter, A., Burrows, J.P., Nuss, H., Granier, C., Niemeier, U., 2005. Increase in tropospheric nitrogen dioxide over China observed from space. Nature 437, 129–132.

Schneider, J., Weimer, S., Drewnick, F., Borrmann, S., Helas, G., Gwaze, P., Schmid, O., Andreae, M.O., Kirchner, U., 2006. Mass spectrometric analysis and aerodynamic properties of various types of combustion-related aerosol particles. Int. J. Mass Spectrom. 258, 37–49.

Seinfeld, J.H., Pandis, S.N., 2006. Atmospheric Chemistry and Physics: from Air Pollution to Climate Change. John Wiley & Sons, INC, New York.

Shim, J.-M., Park, S.-U., 2004. Acidic loadings in South Korean ecosystems by long-range transport and local emissions. Atmos. Environ. 38, 5623–5636.

Streets, D., Tsai, N., Akimoto, H., Oka, K., 2001. Trends in emissions of acidifying species in Asia, 1985–1997. Water, Air, & Soil Pollut. 130, 187–192.

Sueper, D., 2009. ToF-AMS high resolution analysis software. Online available at: http://cires.colorado.edu/jimenez-group/ToFAMSResources/ToFSoftware/index.html. .

Sun, J., Zhang, Q., Canagaratna, M.R., Zhang, Y., Ng, N.L., Sun, Y., Jayne, J.T., Zhang, X., Zhang, X., Worsnop, D.R., 2011a. Highly time- and size-resolved characterization of submicron aerosol particles in Beijing using an Aerodyne Aerosol Mass Spectrometer. Atmos. Environ. 44, 131–140.

Sun, Y.L., Zhang, Q., Schwab, J.J., Demerjian, K.L., Chen, W.N., Bae, M.S., Hung, H.M., Hogrefe, O., Frank, B., Rattigan, O.V., Lin, Y.C., 2011b. Characterization of the sources and processes of organic and inorganic aerosols in New York city with a high-resolution time-of-flight aerosol mass apectrometer. Atmos. Chem. Phys. 11, 1581–1602.

Sunder Raman, R., Hopke, P.K., 2007. Source apportionment of fine particles utilizing partially speciated carbonaceous aerosol data at two rural locations in New York State. Atmos. Environ. 41, 7923–7939.

Ulbrich, I.M., Canagaratna, M.R., Zhang, Q., Worsnop, D.R., Jimenez, J.L., 2009. Interpretation of organic components from positive matrix factorization of aerosol mass spectrometric data. Atmos. Chem. Phys. 9, 2891–2918.

Weimer, S., Alfarra, M.R., Schreiber, D., Mohr, M., Prevot, A.S.H., Baltensperger, U., 2008. Organic aerosol mass spectral signatures from wood-burning emissions: influence of burning conditions and wood type. J. Geophys. Res. Atmos. 113.

Yamaji, K., Li, J., Uno, I., Kanaya, Y., Irie, H., Takigawa, M., Komazaki, Y., Pochanart, P., Liu, Y., Tanimoto, H., Ohara, T., Yan, X., Wang, Z., Akimoto, H., 2010. Impact of open crop residual burning on air quality over Central Eastern China during the Mount Tai Experiment 2006 (MTX2006). Atmos. Chem. Phys. 10, 7353–7368.

Zhang, Q., Jimenez, J., Canagaratna, M., Ulbrich, I., Ng, N., Worsnop, D., Sun, Y., 2011. Understanding atmospheric organic aerosols via factor analysis of aerosol mass spectrometry: a review. Anal. Bioanal. Chem. 401, 3045–3067.